Measurement of the D_α spectrum produced by fast ions in DIII-D

Y. Luo and W. W. Heidbrink
University of California, Irvine, California 92697

K. H. Burrell, D. H. Kaplan, and P. Gohil
General Atomics, San Diego, California 92186

(Received 8 November 2006; accepted 29 January 2007; published online 21 March 2007)

Fast ions are produced by neutral beam injection and ion cyclotron heating in toroidal magnetic fusion devices. As deuterium fast ions orbit around the device and pass through a neutral beam, some deuterons neutralize and emit D_α light. For a favorable viewing geometry, the emission is Doppler shifted away from other bright interfering signals. In the 2005 campaign, we built a two channel charge-coupled device based diagnostic to measure the fast-ion velocity distribution and spatial profile under a wide variety of operating conditions. Fast-ion data are acquired with a time resolution of ~1 ms, spatial resolution of ~5 cm, and energy resolution of ~10 keV. Background subtraction and fitting techniques eliminate various contaminants in the spectrum. Neutral particle and neutron diagnostics corroborate the D_α measurement. Examples of fast-ion slowing down and pitch angle scattering in quiescent plasma and fast-ion acceleration by high harmonic ion cyclotron heating are presented. © *2007 American Institute of Physics.* [DOI: 10.1063/1.2712806]

I. INTRODUCTION

Fast ions in present-day fusion devices are either externally introduced by neutral beam injection or internally generated by ion cyclotron heating and by fusion reactions. Fast ions can be a major source of energy, momentum, and particles for the plasma. Although dilute populations of fast ions often behave classically, intense populations can drive instabilities that redistribute or expel the fast ions from the plasma.[1] Established fast-ion diagnostic techniques[2] include neutron and gamma-ray measurements, neutral-particle analysis, collective scattering, and detection of lost fast ions near the vacuum vessel wall.

Conceptually, a fast-ion D_α (FIDA) diagnostic is a type of charge exchange recombination (CER) diagnostic.[3] Fast helium populations during ^{3}He injection were measured on JET.[4] Alpha particles produced in deuterium-tritium reactions were measured on the tokamak fusion test reactor (TFTR).[5] The first FIDA measurements[6] were made on DIII-D using an existing spectrometer that only measured a portion of the FIDA spectrum. Following those successful measurements, a dedicated instrument[7] was designed to measure the entire spectrum. This article summarizes the performance of this instrument in the 2005 campaign.

The article is organized as follows. Section II summarizes the diagnostic concept and challenges.[6] Section III describes the FIDA instrument[7] and the criteria for selection of the various hardware components. Section IV discusses extraction of the fast-ion signal from the raw data. Estimates of the expected signal are consistent with the measured intensity (Sec. V). Section VI presents some physics results that illustrate the capability of the FIDA diagnostic. Section VII discusses the implications of our operational experience and makes suggestions for further improvements.

II. FIDA CONCEPT

In neutral-beam-heated tokamak plasmas, as deuterium fast ions circulate the device, they can pass through a neutral beam, where some fast ions neutralize by charge exchanging with the injected neutrals. Some of the neutralized fast ions (reneutrals) are in excited states. After traveling a distance in a straight line, the excited state decays by emitting a photon,

$$D^0 + D^+ \Rightarrow D^+ + D^{0*} \Rightarrow D^+ + D^0 + \gamma. \quad (1)$$

D_α light, which is the transition from the $n=3$ to $n=2$ energy level, has a rest wavelength of 656.1 nm. It is in the visible range and can be easily measured with a standard spectrometer, camera, and lens system. The Doppler shift of the D_α line depends on the velocity component of the reneutral along the viewing line. For a CER diagnostic, the emitters (impurity ions) are in thermal equilibrium with the plasma and consequently can be assumed to have a Maxwellian distribution function. As a result, Doppler broadening leads to a Gaussian shaped spectrum. The ion temperature and rotation speed are determined from the Doppler broadening and the er shift of the spectral line, respectively. For a FIDA diagnostic, since fast ions carry much higher energy and have an anisotropic distribution function, the D_α spectrum is much broader and has a non-Gaussian shape. A particular wavelength in the spectrum corresponds to fast ions with a particular velocity component along the viewing line and arbitrary velocity components in the other orthogonal directions.

For a FIDA measurement, avoiding the bright emission from other deuterium neutrals is a major challenge. There are four populations of deuterium neutrals in a typical tokamak plasma.[8] At the plasma edge and pedestal region, there are enormous populations of relatively cold neutrals with a temperature on the order of ~10 eV. These edge neutrals radiate brightly near the rest D_α wavelength. Along the neutral beam

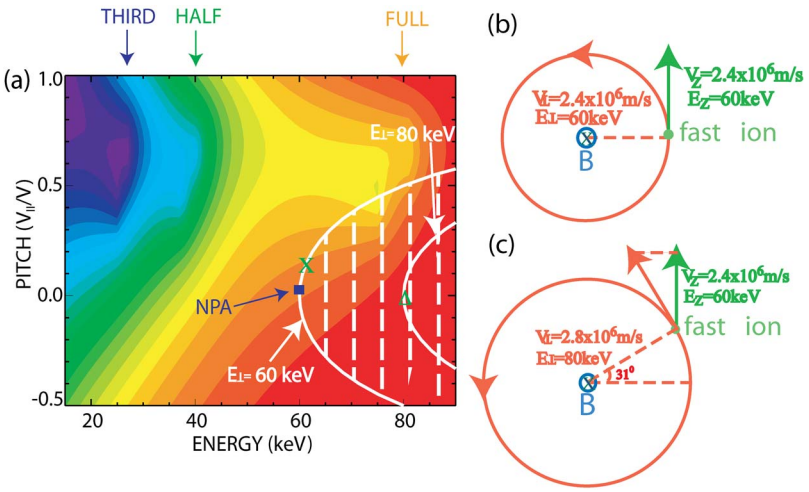

FIG. 1. (Color online) (a) Contour plot of the fast-ion distribution function from a local Fokker-Planck calculation. The two parabolalike curves represent fast ions with 60 and 80 keV perpendicular energies, respectively. The green $X(\Delta)$ indicates velocity coordinates that produce the gyro-orbit shown in panel (b) and (c). Fast ions in the white hatched region may have a vertical velocity of 2.4×10^6 m/s. The blue rectangle shows the velocity space of fast ions detected by a vertical NPA channel at 60 keV. (b) The gyro-orbit of any fast ion on the 60 keV perpendicular energy curve. The vertical energy (E_z) is labeled for a specific gyroangle. (c) The gyro-orbit of any fast ion on the 80 keV perpendicular energy curve. The vertical energy is labeled for a specific gyroangle.

lines, there are injected neutrals with full, half, and third energies. Because of their great velocity (2.8×10^6 ms^{-1} for an 80 keV deuteron), the er shift of the D_α emission can be as large as 6 nm. In addition to the er shift, there is also Stark splitting associated with both the motional $\mathbf{v}\times\mathbf{B}$ Stark effect and plasma electric fields. This splitting can result in ~1 nm spread of the D_α emission from full energy injected neutrals. The third population of neutrals is halo neutrals around the injected beams, which are formed by charge exchange events between injected neutrals and plasma deuterons. The velocity distribution of this population is approximately the local velocity distribution of plasma ions. For an ion temperature of 5 keV, the resulting er shift of the D_α line is around 1.5 nm. These three populations of neutrals constitute the bright interferences for the FIDA diagnostic. The last population of neutrals is what is intended to measure: reneutrals born in charge exchange events from fast ions. Reneutrals have the same energy as fast ions, and as a result, the D_α emission of reneutrals produces a broad feature in the spectrum. The challenge is to separate the FIDA signal from the interfering signals as much as possible. If detector saturation is avoided, the emission from edge neutrals and halo neutrals poses few difficulties because it only spans a small portion of the wavelength range of interest and that portion of the wavelength range corresponds to low energy fast ions. However, the emission from injected neutrals could be devastating due to the potentially large er shift and Stark effect. There are two ways to overcome this hurdle. One is to only use the half of the spectrum which is uncontaminated by injected neutrals. If the emission from injected neutrals is blue- (red-) shifted, then the red (blue) side of the spectrum is taken. The other way is to view the neutral beam perpendicularly. This favorable viewing geometry eliminates the er shift of the emission of the injected neutrals, and thus all three interfering signals sit in a small range around the rest D_α wavelength. All three bright interfering signals can be blocked by a bar at the exit focal plane of the spectrometer, as discussed later.

Removing the background from visible bremsstrahlung and scattering is another challenge for a FIDA measurement. Visible bremsstrahlung spreads uniformly over the entire range of interest and scales as n_e^2. On the other hand, the FIDA signal decreases with increasing n_e.[6] In a high density discharge in DIII-D, visible bremsstrahlung could be an order of magnitude stronger than the FIDA signal. Even in a typical low density discharge, the visible bremsstrahlung and FIDA signals are comparable. Thus, it is essential to do precise background subtraction. This is achieved through modulation of the injected neutral beam in a steady plasma, which can be done routinely in DIII-D. In a transient plasma, changes in background must be independently monitored.

Figure 1 illustrates the relationship between the observed er shift and the fast-ion distribution function. Because of the rapid gyromotion, in a strongly magnetized plasma, the fast-ion distribution function only depends upon two velocity coordinates. (The phase of the gyroangle is an ignorable coordinate.) A common choice of velocity coordinates is energy and the pitch of the velocity vector relative to the magnetic field. Figure 1(a) illustrates a typical fast-ion distribution in a beam-heated DIII-D discharge as a function of energy and pitch. Neutral beams inject deuterons with a particular angle with respect to the magnetic field at three distinct energies. Coulomb scattering decelerates the injected fast ions and scatters them in pitch, filling in the distribution. The er shift of a FIDA photon provides information on one component of the fast-ion velocity vector. A reasonably straightforward interpretation of the signal is available for the vertically viewing geometry employed in our DIII-D installation. The measured velocity component is (approximately) perpendicular to both the injected beam and the magnetic field. Consider the Doppler shift that corresponds to a vertical velocity of 2.4×10^6 m/s in the direction of the detector. Figures 1(b) and 1(c) illustrate the gyromotion of two ions that could produce this Doppler shift. The minimum perpendicular energy that could produce this Doppler shift is 60 keV [Fig. 1(b)]; in this case, the ion produces the desired Doppler shift if it neutralizes just as it is traveling toward the detector (at the 0° gyroangle). The Doppler shift can also be produced by a higher energy ion; Fig. 1(c) shows the gyrophase of an ion with a perpendicular energy of 80 keV that has the correct vertical velocity component if it neutralizes at a gyroangle of 31°. In addition to the two velocity components illustrated in Figs. 1(b) and 1(c), there is a third velocity component: the component parallel to the magnetic field. This component does not affect the perpendicular gyromotion, so as long as

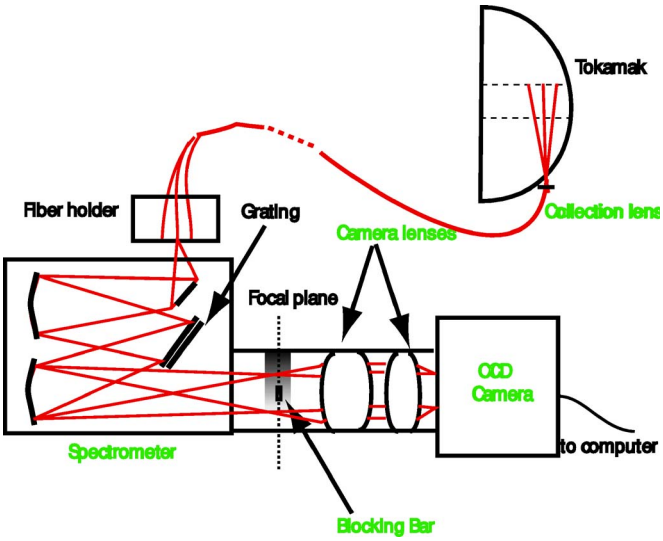

FIG. 2. (Color online) FIDA system schematic as viewed from above. The shaded rectangle represents the dispersion of wavelength.

they have the correct perpendicular energy, particles with any value of parallel energy can also contribute light at the selected Doppler shift. In terms of energy E and pitch p, any ion that satisfies the equation

$$E = E_{\perp}/(1 - p^2) \tag{2}$$

can also contribute light at the selected Doppler shift. (Here $E_{\perp}$ is the perpendicular energy that corresponds to 60 keV in this example.) As illustrated in Fig. 1(a), any ions on the 60 keV perpendicular energy curve and in the enclosed hatched region can contribute to the selected wavelength as long as the charge exchange event happens at the proper gyroangle. Thus, for vertical views, the FIDA signal at a particular wavelength originates from an effective average over perpendicular energy.

The observed spectral shape results from a convolution of the fast-ion velocity distribution with atomic rates, particularly the energy dependent charge-exchange rate. Views perpendicular to the injected neutral beam are less sensitive to spectral distortion by atomic effects than tangential views.[6] Ignoring the atomic effects, Egedal and Bindslev[9] have considered the relationship between measurements of one velocity component and the gyrotropic fast-ion velocity distributions that occur in magnetized plasma. They show that, although a unique inversion from the measurements to the distribution functions is impossible, salient features of the distribution can be reliably inferred. In practice, forward modeling that follows fast ions from an assumed distribution function through all relevant atomic processes simulates the expected spectrum.[6] In quiet plasmas, simulations employing the fast-ion distribution function predicted by TRANSP are in excellent agreement with the measured spectra. These comparisons will be the subject of a future publication.

III. HARDWARE DESCRIPTION

Figure 2 shows a schematic view of the FIDA system. The D_{α} light of reneutrals is emitted from the region of plasma traversed by the neutral beam (reneutrals usually travel less than 5 cm before they radiate). A lens ($f/4.4$) located at a port under the midplane collects and focuses light onto several optical fibers with a 1500 μm core diameter, each of which defines a viewing chord through the plasma. The observation volume of each chord can be approximated by a cylinder across the beam. The light travels along the optical fibers to a Czerny-Turner spectrometer ($f/4$, 1800 grooves/mm grating, and 300 mm focal length) with a fiber holder mounted around the entrance slit. The FIDA diagnostic is designed to accommodate two channels simultaneously with the ability to switch fibers between discharges. Fibers can be switched quickly at the fiber holder if necessary. At the exit plane of the spectrometer, the light is dispersed into a two dimensional pattern: vertically, the light is separated into two chords; horizontally, the light from each fiber is dispersed in wavelength (as indicated by the shading in the focal plane shown in Fig. 2). A vertical bar sitting on two horizontal translation stages on the exit focal plane blocks the portion of the spectrum with bright interfering signals that would otherwise saturate the detector. The blocking bar has a rectangular cross section 1 mm wide and 2 mm long. The bottom of the bar is threaded so that the bar can be rotated and has an adjustable blocking range between 1 and $\sqrt{5}$ mm. We typically block a 2 nm portion of the D_{α} range. The image on the exit focal plane is reduced by two camera lenses (85 and 50 mm focal lengths) coupled together by a macrocoupler and a step ring. A charge-coupled device (CCD) camera (2.2 MHz, 14 bits) with its CCD chip (8×6 mm^2) on the focal plane of the second lens detects the light with 1 ms integration time. The CCD camera is surrounded by a radiation shielding box (discussed later). Electrical signals from the CCD chip are amplified, digitized, and transferred to a dedicated Windows personal computer (PC). The data are then transferred to a master Linux PC through Ethernet cable. Finally, they are archived to the DIII-D data server.

The FIDA diagnostic is designed with maximum light gathering power at the D_{α} wavelength, subject to the constraint of matching the optics on the tokamak. With an $f/4.4$ collection lens, fixed CCD chip width, and constant spectral resolution, the detected signal is independent of the f/number of the spectrometer if light loss from lens surfaces is ignored. However, if the f/number of the spectrometer does not match the f/number of the collection lens, two lenses are needed in front of the entrance slit to convert the f/number, which increases the complexity of the system and leads to loss of some portion of light. Thus a spectrometer of $f/4$ is optimal for the FIDA diagnostic. Another important specification of the spectrometer is the groove density of the grating in the spectrometer. Assuming constant spectral resolution, the higher the groove density, the wider the entrance slit can be, which translates into more signal detected. The groove density is subject to two constraints. The first one is dispersion. If dispersion is too high, we have trouble demagnifying the image to fit onto the CCD chip. Since the lowest f/number of readily available commercial lenses is $f/1$, the largest demagnification ratio we could achieve is 1/4 with $f/4$ and $f/1$ lenses. The second constraint is the optimum range of operation for the grating. Generally high groove density gratings

are optimized for short wavelength. Based on the above considerations, SpectraPro 300i from the Acton Research Corporation ($f/4$, 1800 grooves/mm grating, and 300 mm focal length) was chosen.

The bright interfering signals around the rest D_α wavelength require an extremely high dynamic range for the detector, which usually comes at a very high cost. There are three possible solutions. A notch filter would be ideal and easy to integrate into the system (it could be put between the two camera lenses). The problem with this solution is that the width of the required filter is too narrow (2 nm). Such notch filters are not commercially available yet. Oversampling very rapidly could be a solution, but it would require unrealistic CCD speed. Moreover the camera readout noise would be huge if the camera ran so fast. A practical expedient is to use a blocking bar on the exit focal plane of the spectrometer. The blocking is positioned to block the interfering light.

The image on the exit focal plane of the spectrometer is about 11 mm wide, which exceeds the width of the CCD chip (8 mm). Therefore an image reducer with a demagnification ratio of 8/11 or smaller is required between the spectrometer and the CCD camera. Although simple lenses do not have a flat focal plane, camera lenses are compound, multielement lenses specifically designed to create a flat image on a piece of film or a flat CCD chip. Another advantage of camera lenses is that they are relatively inexpensive because of the mass consumer market. Theoretically either one single lens or a pair of lenses can serve as an image reducer; however, two coupled lenses can substantially improve the quality of image. The two camera lenses are subject to three constraints. First, the ratio of the focal lengths of the lenses should be 8/11 or a little less to ensure that the full D_α spectrum can be detected by the camera. Second, the first lens should be capable of collecting all the D_α light coming out of the spectrometer. This means the lens should have an f/number equal to or lower than the f/number of the spectrometer ($f/4$). Third, the aperture of the second lens should be large enough to collect all of the light that comes out of the first lens. Nikkor 85 mm $f/1.8$ AF and Nikkor 50 mm $f/1.4$ AF meet the above requirements and are chosen for the image reducer.

The fast-ion profile can change on an $\sim$1 ms time scale. Consequently the FIDA diagnostic is designed to have a minimum integration time of 1 ms. Another benefit of such a high temporal resolution is that data contaminated by edge localized modes (ELMs) can be identified and removed (as is discussed in Sec. IV). Unfortunately it is hard to find a shutter capable of operating this fast. In order to take multiple spectra on a single CCD camera without a shutter, there have to be multiple readout nodes to read out the spectra separately to avoid cross talk. The CCD camera chosen is the VelociCam™ VC105A from PixelVision™ which has four readout nodes. It can take two spectra with one on the upper half of the CCD chip and one on the lower half of the CCD chip. If each spectrum can be reduced to half of the CCD width, the camera can take four spectra simultaneously. The FIDA diagnostic is designed to take two spectra to get more signal and facilitate the design of the blocking component. Since the vertical direction of each spectrum on the CCD chip contains no useful information, pixels on the vertical direction are binned together to improve the readout speed. In addition, since only a coarse spectral resolution is necessary, the serial direction bins by two. When operating under the above binning, a minimum integration of 0.33 ms is achieved, which exceeds the 1 ms requirement.

The CCD camera is very sensitive to neutron/γ radiation, especially γ rays. Neutrons are produced by fusion reactions in the DIII-D plasma and the subsequent production of γ rays occurs by neutron capture in the surrounding structure. The FIDA camera is located outside the DIII-D neutron shield wall. To introduce further neutron/γ shielding, a shielding box[10] is put around the CCD camera. The shield has shielding material on five sides, with the spectrometer being on the sixth, open side which faces away from the tokamak. For each side, 15 cm of borated polyethylene and 5 cm of lead are used to absorb neutrons and γ rays, respectively. This provides about a factor of 40 reduction in the n/γ hits on the detector.

Three timing triggers are required for the FIDA diagnostic. The CCD camera trigger commands the camera to read out data. The camera is triggered every 1 ms during each shot to have a 1 ms integration time and every 10 ms between shots to keep the temperature of the camera stable. The camera is connected to the slave Windows PC. The slave PC is triggered a short time before each shot to start transferring data from the camera to the PC. The master Linux PC which remotely controls the camera also needs a trigger before each shot to get ready for transferring data from the slave PC to the master PC. The PCI-6601 timing card from National Instruments is inserted into the slave PC and configured to generate various trigger pulses. The PCI-6601 timer/counter has four counters. A timing pulse from the timing receiver, synchronized with DIII-D operations, provides input to the counters. The first counter is configured to generate retriggerable single pulses, which are input for the second counter. The second counter, which performs frequency shift keying, produces pulses every 1 ms during a shot and every 10 ms between shots. The output of the second counter serves as the camera trigger. The third counter, which is configured to generate retriggerable single pulses, provides the timing trigger for the slave PC. The timing trigger for the master PC can be generated similarly by the fourth counter. In reality, a timing pulse from the timing receiver is used to trigger the master PC directly.

IV. EXTRACTION OF THE FAST-ION SIGNAL FROM THE SPECTRUM

Figure 3(a) shows typical raw data. There are various contaminants in the spectrum. Impurity lines appear as bumps in the spectrum. Halo emission extends beyond the blocked wavelengths on both sides. Visible bremsstrahlung and scattered light are distributed over the entire spectrum and are most evident beyond the injection energy, where no fast-ion signal is expected in the absence of ion cyclotron heating. Finally, for some time slices, there are huge spikes caused by neutron or gamma hits.

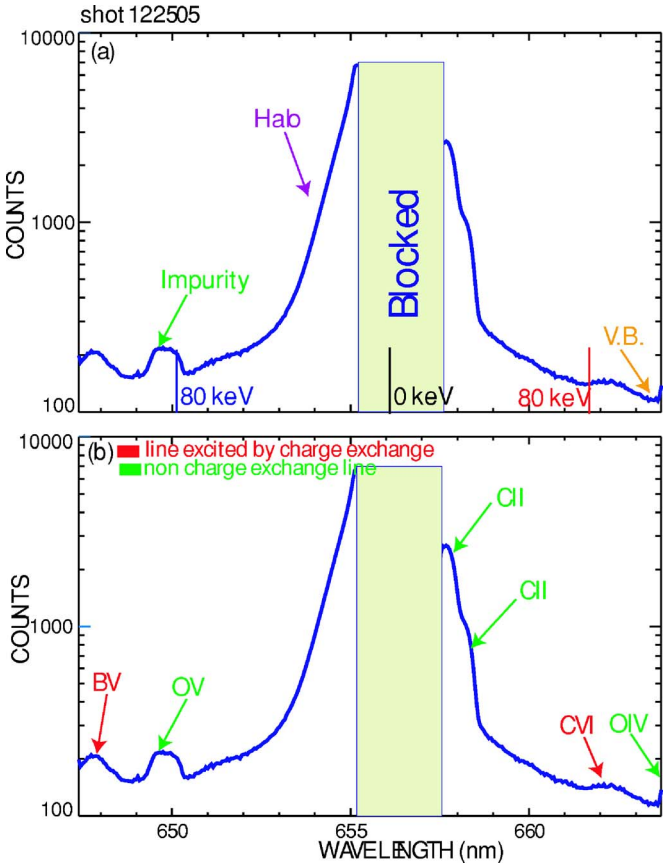

FIG. 3. (Color online) (a) Contaminants in the spectrum. A log plot is shown in order to make impurity lines, visible bremsstrahlung, and scattered light clearer. The central part of the spectrum is blocked by the blocking bar to avoid saturation. (b) Impurity lines in the spectrum.

Although the CCD camera is placed inside the shielding box, neutrons and gamma rays can penetrate to the CCD chip occasionally, especially when the discharge has a neutron rate in excess of 10^{15} n/s. Neutron/gamma hits affect one pixel (or two pixels when the hit occurs on the boundary of pixels). They usually appear as huge spikes (at least hundreds of counts) that are readily identified and replaced by the average of the adjoining pixels. Small spikes caused by neutron/gamma hits on the sharply rising or falling slope of halo emission are more challenging to detect; a special conditional statement in the code identifies these hits.

Figure 3(b) shows a detailed look at the impurity lines. There are six main impurity lines in the spectrum. The BV and CVI lines are lines excited by charge exchange; they appear only when the FIDA beam is on. The OV line, the two CII lines, and the OIV line are noncharge exchange lines. They appear whether the beam is on or not, and therefore, they can be removed by beam modulation and time slice subtraction.

Impurity lines are removed by fitting a theoretical response function to the data using the method of nonlinear least squares. The impurity line is a Gaussian due to Doppler broadening (assuming a Maxwellian distribution function). The theoretical response function is the convolution of the Gaussian line shape radiated by the impurity with the instrumental response. In general, convolution needs to be done numerically; however, the convolution of two Gaussians is

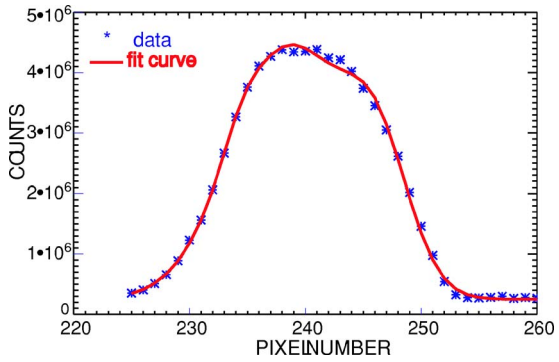

FIG. 4. (Color online) Spectrum from a calibration lamp showing the fitting of the instrumental response [Eq. (3)].

another Gaussian. This is the motivation for us to represent the instrumental response by the sum of a few Gaussians. The instrumental response data are taken by illuminating the fibers with a neon lamp. Because neon is cold, Doppler broadening of such lines is negligible, thus the broadening observed in such a measurement is only due to instrumental effects. We have determined empirically that the instrumental response function can be adequately represented by the sum of three Gaussians (Fig. 4),

$$I_i = \sum_{j=1}^{3} \frac{a_j}{\sigma_j \sqrt{2\pi}} \exp\left[-\frac{(i-\mu_j)^2}{2\sigma_j^2} \right]. \tag{3}$$

Here, i denotes the pixel number, j denotes different Gaussians, a_j is the amplitude, σ_j is the standard deviation, and μ_j is the center location. Assuming the Gaussian line radiated by the impurity due to Doppler broadening is

$$I_i = \frac{a}{\sigma \sqrt{2\pi}} \exp\left[-\frac{(i-\mu)^2}{2\sigma^2} \right], \tag{4}$$

the theoretical response function for the impurity line is

$$I_i(a,\sigma,\mu) = \sum_{j=1}^{3} \frac{a_j a}{\sqrt{\sigma_j^2 + \sigma^2}\sqrt{2\pi}} \exp\left[-\frac{(i-\mu_j-\mu)^2}{2(\sigma_j^2+\sigma^2)} \right]. \tag{5}$$

The empirical approximation of a straight line suffices for the fast-ion contribution in the short spectral range that the impurity line spans,

$$I_i = c_1 + c_2 i. \tag{6}$$

The complete theoretical response function including impurity contribution and fast-ion contribution is

$$I_i(a,\sigma,\mu,c_1,c_2) = \sum_{j=1}^{3} \frac{a_j a}{\sqrt{\sigma_j^2 + \sigma^2}\sqrt{2\pi}} \times \exp\left[-\frac{(i-\mu_j-\mu)^2}{2(\sigma_j^2+\sigma^2)} \right] + c_1 + c_2 i. \tag{7}$$

This theoretical function with five free parameters is fitted to the experimental data by MPFIT,[11] which uses the Levenberg-Marquardt technique[12,13] and has the capability of imposing boundary constraints on parameter values. After the fitting is completed, the impurity line contribution [which is the three Gaussians in Eq. (7)] is subtracted from the raw data (Fig. 5).

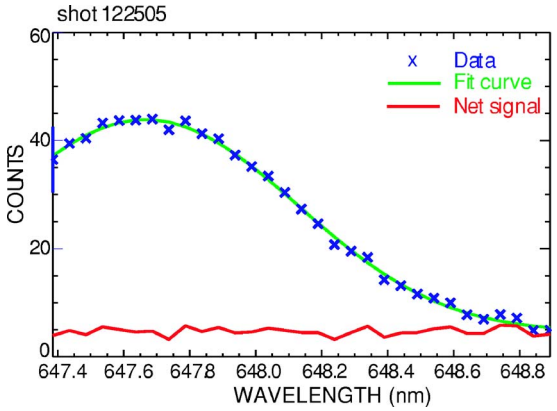

FIG. 5. (Color online) Fitting of the BV line. The fast-ion signal is near zero because this impurity line is in the wavelength range which corresponds to energies above the injection energy.

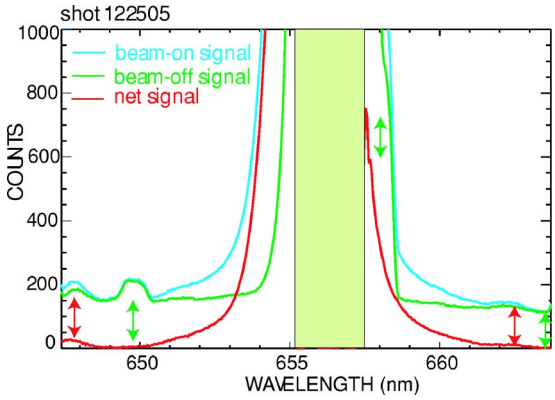

FIG. 7. (Color online) Background subtraction by means of beam modulation. The beam is modulated with 10 ms on and 10 ms off. The beam-on and beam-off signals in this figure are averaged over a 300 ms time window.

Theoretically, the halo signal can be removed using the same fitting technique since the halo signal can be modeled the same way as impurity lines; however, it is much harder to fit the halo signal. One difficulty is that the halo signal spans a much broader range than impurity lines and the central part is blocked. Another difficulty is that the fast-ion contribution is substantial over the same range. Thus, building an accurate fast-ion model is crucial. Unfortunately, no universal fast-ion model exists since the line shape depends on plasma conditions. We employ an *ad hoc* three parameter polynomial as the fast-ion model and get reasonable fits (Fig. 6). The ion temperature at the chord location derived from halo fitting is 6 keV, in very rough agreement with the CER measurement of carbon impurities of 4 keV. A rough estimate shows that the halo signal can only reach as far as 20 keV in the spectrum in a plasma with a temperature of 4 keV. This means that the fitting is not even necessary with moderate ion temperature plasmas since the low energy fast ions are not of particular interest. However, in extremely high temperature plasmas, the halo signal can contaminate a larger range and halo fitting becomes important. Therefore, finding a good fast-ion model would be beneficial.

Beam-on and beam-off subtraction is an important technique to remove contaminants in plasmas that evolve slowly relative to the time between beam pulses. Visible bremsstrahlung, some scattered light, and noncharge exchange impurity lines are readily eliminated. As shown in Fig. 7, the four noncharge exchange impurity lines completely disappear. Visible bremsstrahlung and scattered light are also well subtracted, as can be seen from the wings of the spectrum above the injection energy. This subtraction is usually done over a selected time window. To study fast ions in quiescent plasma, large windows (a few hundreds of milliseconds) are selected to improve the signal to noise ratio.

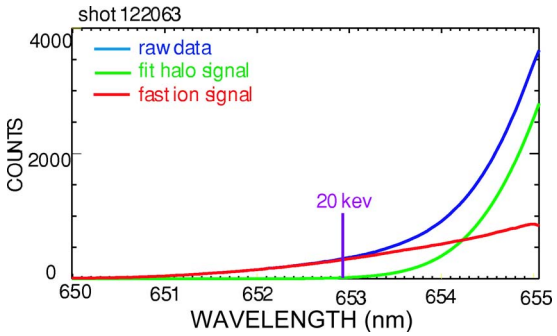

FIG. 6. (Color online) Fitting of halo signal. The result is shown as two components (halo contribution and fast-ion contribution). The line shows the wavelength corresponding to 20 keV energy. Beyond this line on the left side are higher energies. Plasma ion temperature at the chord location for this shot is 4 keV.

Background subtraction by beam modulation works well in many cases but, when there are rapid changes in background, it becomes problematic and special care is required. A common rapid background change for the FIDA diagnostic is caused by ELMs which occur in the high-confinement mode. Since the FIDA sight lines cross the plasma edge, it is not surprising that large ELMs can elevate the FIDA signal significantly through light that scatters off the blocking bar. One ELM can affect up to three time slices depending on the duration of the ELM. As a result, the affected time slices must be eliminated. ELMs are monitored by an independent edge D_α diagnostic at DIII-D. An edge D_α signal is integrated over every 1 ms, which is the FIDA integration time. Empirical absolute and relative thresholds are set to eliminate data contaminated by ELMs. This technique works well in steady-state *H*-mode plasmas with occasional ELMs.

After the background subtraction, there are two impurity lines remaining (BV and OVI). They are fitted and removed from the spectrum, as described above. For plasmas with steady conditions, the combination of beam modulation, fitting of charge-exchange lines, and removal of time slices that are contaminated by occasional bursts of edge D_α light successfully extracts the fast-ion signal from the measured spectra.

On the other hand, the beam-modulation technique is inadequate for transient plasmas. An important application of the FIDA diagnostic is to measure the effect of transient instabilities on the fast-ion distribution. These instabilities often expel particles or heat to the plasma edge, causing changes in background that can obscure the fast-ion contribution to the spectrum. Analysis of these plasmas requires removal of backgrounds from individual time slices. The first step of the analysis is to fit and remove the impurity lines, as

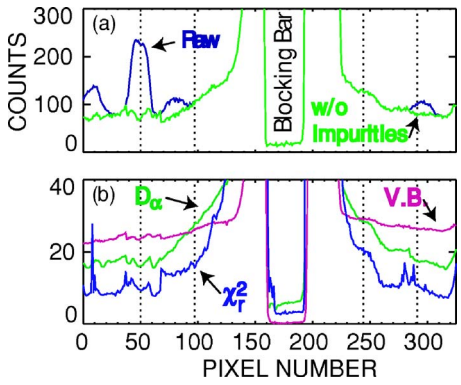

FIG. 8. (Color online) (a) A typical background spectrum before and after removal of the impurity lines. The data are from the discharge shown in Fig. 11 between 3141 and 3149 ms. (b) Fit coefficients a_V and a_D vs pixel number obtained from multiple regression on a database of over 4000 background spectra. Also shown is the reduced chi square of the fit. The dotted vertical lines indicate wavelengths that correspond to vertical energies of 30 and 80 keV.

described above. Next, we assume that visible bremsstrahlung and scattered cold D_α light, are the dominant contributions to the remaining background, so

$$B = a_V V + a_D D, \tag{8}$$

where B is the background, V is the magnitude of the visible bremsstrahlung, D is the magnitude of the cold D_α light, and a_V and a_D are coefficients that may be functions of wavelength. (Spectra acquired without plasma show that electronic offsets are negligible.) To find a_V and a_D, a large database of background spectra (acquired when the FIDA beam is off) is assembled. Independent measurements of the level of the visible bremsstrahlung V and the cold D_α light D at the times of these spectra are obtained from other DIII-D diagnostics. (Ideally, these quantities would be available along the same sight line as the FIDA chords.) A multiple regression on these background signals yields a_V and a_D for each pixel. The results of this analysis are shown in Fig. 8(b). As expected, the fit coefficient a_V of the visible bremsstrahlung is nearly independent of pixel number, as the dependence of bremsstrahlung on wavelength is weak over this relatively small range of wavelengths. In contrast, the fit coefficient a_D for the cold D_α light is largest near the unshifted D_α line, indicating that scattered light is most important near the central line. Figure 8(b) also shows the reduced chi-squared χ_r^2 of the fit as a function of pixel number. For all wavelengths, χ_r^2 is much larger than unity, indicating that the simple model of Eq. (8) is unable to account for all of the observed variation in background. Investigation of different discharges shows that, on a particular discharge, the optimal fit coefficients a_V and a_D deviate systematically from the average fits. The likely explanation for this is that the available reference bremsstrahlung and D_α signals V and D have a different view of the edge plasma than the FIDA sight lines, so changes in the proportionality coefficients with plasma shape degrade the quality of the fits. Two other features of the χ_r^2 graph are noteworthy. First, the model does a poor job of fitting the background spectra near the blocking bar but this wavelength region is unimportant for fast-ion physics. Second, the value of χ_r^2 often jumps upward in the vicinity of impurity lines, suggesting slight imperfections in the impurity fitting. Overall, however, the fits are smooth and reasonable for the wavelengths of interest. For a typical low-density discharge ($n_e = 2 \times 10^{13}$ cm^{-3}), approximately 65% of the background in the wavelengths of interest is contributed by scattered cold D_α light, with the remaining 35% attributable to visible bremsstrahlung. At higher densities, the visible bremsstrahlung becomes the dominant component of the background, since bremsstrahlung is proportional to n_e^2.

In an actual discharge with transient changes in background, the background for each pixel is taken as

$$B(\lambda,t) = c[a_V(\lambda)V(t) + a_D(\lambda)D(t)]. \tag{9}$$

The scale factor c, which is generally close to unity, is obtained from backgrounds near the time of interest in the particular discharge under investigation and partially corrects for the systematic variations in background associated with changes in plasma shape. An example of dynamic background subtraction is shown in Sec. VI.

V. SIGNAL LEVEL AND SIGNAL TO NOISE RATIO

The spatial calibration and intensity calibration are done when the tokamak is vented to atmosphere. A spatial calibration is performed to determine the spatial location of FIDA measurements for each chord. First, an alignment target is suspended inside the tokamak along the centerline of the viewed neutral beam. Then a neon lamp is placed on the fiber end away from the tokamak to shine backwards through the fiber and collection lens system. The spot where the light illuminates the alignment target is marked and measured. Next, an intensity calibration is completed to convert digitizer counts to number of photons. An integrating sphere source which illuminates over a broad wavelength range with a calibrated spectral radiance is placed on the spot from the spatial calibration and a spectrum is taken by the FIDA instrument with the same settings as for actual discharges.

The number of photons detected by the collection lens in each wavelength bin (pixel) for each chord during the intensity calibration is

$$P \approx L_\lambda A \cos\theta \Omega \Delta\lambda \Delta T, \tag{10}$$

where L_λ is the spectral radiance of the integrating sphere source in photons cm^{-2} sr^{-1} nm^{-1} s^{-1}, A is the source area viewed by the chord on the alignment target in cm^2, θ is the angle between the alignment target surface normal and the viewing direction, Ω is the solid angle subtended by the collection lens, $\Delta\lambda$ is the wavelength bin for the pixel in nm, and ΔT is the integration time in s. P is a function of wavelength or pixel since L_λ is a function of wavelength. The number of digitizer counts induced by the integrating sphere is the count difference between the intensity calibration shot and a dark shot. The conversion factor in photons count^{-1} is calculated by dividing the number of digitizer counts from the number of photons for each pixel. For the innermost FIDA chord, the conversion factor is approximately 180 for all the pixels.

The absolute signal level in terms of the number of photons can be determined by multiplying the number of digitizer counts by the conversion factor pixel by pixel and sum-

ming. It can also be estimated based on the fast-ion density, neutral density, atomic data, and geometric parameters. In order to compare the estimated signal level with experimental data, a discharge with a quiet plasma is selected. The fast-ion signal in digitizer counts is extracted from the raw data first as discussed in Sec. IV. The measured signal level in photons is obtained by multiplying the fast-ion signal and the conversion factor. Since the middle portion of the spectrum is blocked, we only calculate the signal level beyond 20 keV. The result is 2.6×10^6 photons. This is the number of D_α photons from neutralized fast ions entering into the collection lens in 1 ms.

The signal in number of photons can be estimated independently by the following formula:

$$s \approx f_{>20} n_f n_n \langle \sigma v_{\mathrm{rel}} \rangle V t \left(\frac{\nu_{3-2}}{\sum \nu_{3-n}} \right) \left(\frac{\Omega}{4\pi} \right), \tag{11}$$

where n_f is the fast-ion density and n_n is the neutral density. The factor $f_{>20}$ is the fraction of the fast-ion population with vertical energy greater than 20 keV. It depends on the fast-ion distribution function. The reactivity $\langle \sigma v_{\mathrm{rel}} \rangle$ is the averaged rate coefficient for generating reneutrals in the $n=3$ state, V is the observation volume, t is the integration time, ν_{3-2} is the radiative transition rate from $n=3$ to $n=2$, ν_{3-n} is the reaction rate from $n=3$ to various states including both radiative transition and collisional transition, and Ω is the solid angle subtended by the collection lens. For the quiet discharge we have calculated the measured signal in photons for $f_{>20}\approx 11\%$, $n_f \approx 4.8\times10^{12}$ cm^{-3}, $n_n \approx 1.4\times10^9$ cm^{-3}, and $\langle \sigma v_{\mathrm{rel}} \rangle \nu_{3-2}/\Sigma\nu_{3-n} \approx 1.0\times10^{-9}$ cm^3 s^{-1},[14] so the estimated signal level is around 1.4×10^6 photons, which is reasonably close to the FIDA measurement. A more rigorous calculation of the signal level from the FIDA simulation code that includes all relevant atomic physics effect[6] gives 2.4×10^6 photons, agreeing very well with the FIDA measurement.

Both random errors and systematic errors appear in the FIDA measurements. Random errors include photoelectron noise, readout noise, and dark noise. Photoelectron noise refers to the inherent natural variation of the incident photon flux on each CCD pixel; it equals the square root of the number of collected electrons. The number of collected electrons is the product of the signal in digitizer counts and the gain, which is 2.93 electrons/count when the camera operates at high gain. Readout noise refers to the uncertainty introduced during the process of quantifying the electronic signal on the CCD. It is about 15 electrons at a 0.5 MHz digitizing rate. Dark noise arises from the statistical variation of thermally generated electrons within the silicon layers comprising the CCD. It is reduced dramatically when operating at low temperatures and is proportional to the integration time. Since the PixelVision CCD camera is thermoelectrically cooled and the integration time is 1 ms, dark noise is negligible in the FIDA measurements. The signal to noise ratio (SNR) is given by

$$\mathrm{SNR} = \frac{gN_c}{\sqrt{gN_c + N_r^2}}, \tag{12}$$

where g is the gain, N_c is the digitizer counts, and N_r is the readout noise. The SNR is a function of wavelength. For the pixels on the two wings of the spectrum, N_c is on the order of 100 and photoelectron noise is comparable to readout noise. For the central pixels, N_c is on the order of 1000 and photoelectron noise becomes dominant. The above calculation is for raw data. For steady plasmas, the fast-ion signal is extracted by averaging beam-on and beam-off signals in a chosen time window and doing background subtraction. Assuming N_{on} is the average number of beam-on signals in counts, N_{off} is the average number of beam-off signals in counts, and N_t is the number of time slices averaged for beam on and beam off, the fast-ion signal in electrons is

$$S_{\mathrm{fi}} = g(N_{\mathrm{on}} - N_{\mathrm{off}}). \tag{13}$$

The standard deviation of averaged beam-on signals in electrons is

$$\sigma(\mathrm{on}) = \frac{\sqrt{gN_{\mathrm{on}} + N_r^2}}{\sqrt{N_t}}. \tag{14}$$

The standard deviation of averaged beam-off signals in electrons is

$$\sigma(\mathrm{off}) = \frac{\sqrt{gN_{\mathrm{off}} + N_r^2}}{\sqrt{N_t}}. \tag{15}$$

Adding the above two contributions in quadrature, we obtain the standard deviation of the net signal (fast-ion signal), which is

$$\sigma(\mathrm{fi}) = \sqrt{\frac{g(N_{\mathrm{on}} + N_{\mathrm{off}}) + 2N_r^2}{N_t}}. \tag{16}$$

The signal to noise ratio is

$$\mathrm{SNR} = \sqrt{N_t}\frac{g(N_{\mathrm{on}} - N_{\mathrm{off}})}{\sqrt{g(N_{\mathrm{on}} + N_{\mathrm{off}}) + 2N_r^2}}. \tag{17}$$

Not surprisingly, the signal to noise ratio is better for the central pixels since the difference between the beam-on and beam-off counts is much larger. To improve the signal to noise ratio for a certain pixel, we can average our signal over a larger time window. However, the above formula assumes that there are only random errors. This holds true approximately in quiescent plasmas. In plasmas with instabilities, dynamic changes in background introduce systematic errors that invalidate large time windows. Systematic errors strongly depend on plasma conditions and should be addressed case by case.

An example of random errors in a quiescent plasma is shown in Fig. 9. Typically, random errors are small compared to systematic uncertainties associated with background subtraction.

VI. SAMPLE RESULTS

The energy resolution of the FIDA diagnostic is primarily determined by line broadening associated with the motional Stark effect and the slit width of the spectrometer. The

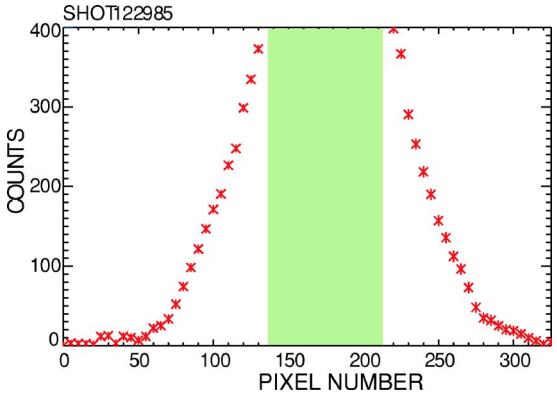

FIG. 9. (Color online) Random error bars. The error bars are calculated using Eq. (16) with $N_t=10$.

motional Stark effect is proportional to $\mathbf{v}\times\mathbf{B}$, where $\mathbf{v}$ is the velocity of reneutrals and $\mathbf{B}$ is the magnetic field. In DIII-D, the degradation in energy resolution caused by the motional Stark effect is about 6 keV. The entrance slit of the spectrometer is opened up to 500 μm to get more signal, which translates into a spectral resolution of ~0.7 nm and an energy resolution of ~8 keV. The overall energy resolution is estimated to be ~10 keV. This estimation is confirmed by the experimental data. As shown in Fig. 1, fast ions are born with full (80 keV), half (40 keV), and third energy (27 keV) components. Through Coulumb collisions with ions and electrons, fast ions experience slowing down and pitch angle scattering and form a fast-ion distribution. In Fig. 10, "steps" in the fast-ion distribution function from half and third energy components are clearly resolved, which demonstrates that the energy resolution of this diagnostic is indeed ~10 keV.

The FIDA diagnostic takes data every 1 ms. To assess the capability of the diagnostic to observe changes in fast ions on a 1 ms time scale, we choose an instability called the sawtooth. A rapid sawtooth crash occurs in less than 1 ms and redistributes fast ions[1] from the core of the plasma to outside the $q=1$ surface; after the crash, the fast-ion density

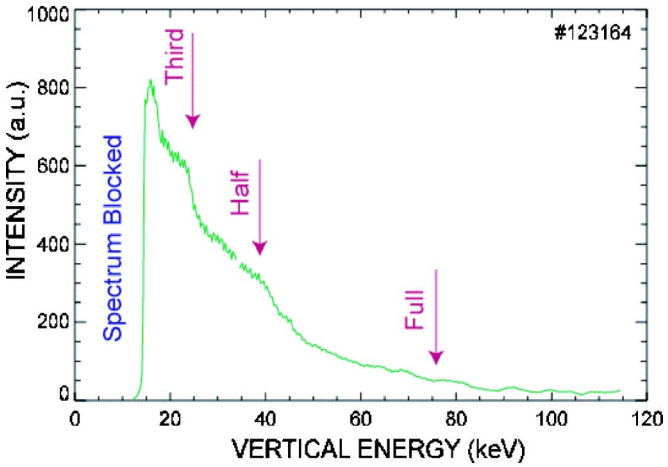

FIG. 10. (Color online) "Steps" in the fast-ion spectrum. The first one is caused by fast ions from the third energy beam component (27 keV). The second one is caused by fast ions from the half energy beam component (40 keV). In the abscissa, wavelength is converted to the equivalent vertical energy that produces the observed Doppler shift.

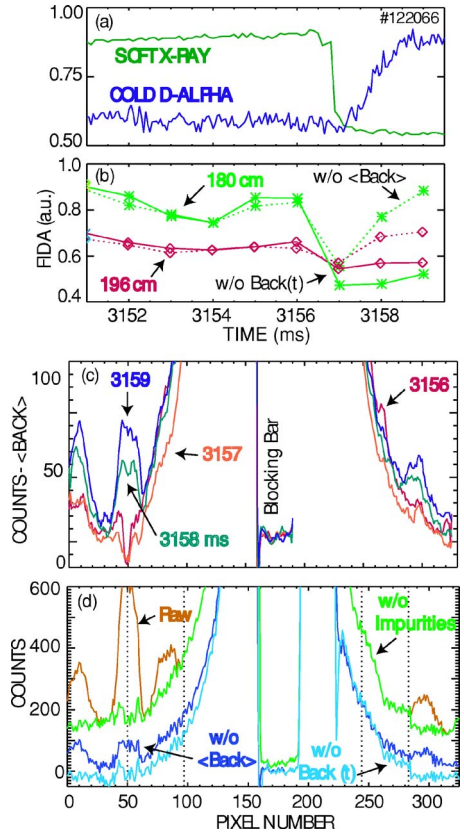

FIG. 11. (Color online) Time evolution of (a) soft x-ray signal and cold edge D_α signal and (b) FIDA signals from two chords after integration over wavelength. The solid lines employ dynamic background subtraction [Eq. (9)], while the dashed lines use the background obtained from beam modulation. (c) Spectra from the central chord at four different times. The average background from the beam-off phase between 3141 and 3149 ms is subtracted from the raw spectra. (d) Spectra from the central chord at 3159 ms. The raw data, data with fitted impurity lines removed, data with the average background subtracted, and data with fitted impurity lines and dynamic background subtracted [Eq. (9)] are all shown. Discharge conditions: line-average electron density of 2.0×10^{13} cm^{-3}; beam power of 3.8 MW.

recovers on a relatively slow time scale ($\geqslant$10 ms). In Fig. 11(a), the quick drop of the soft x-ray signal at 3157 ms indicates a sawtooth crash. The sawtooth causes a heat pulse to propagate from the plasma interior to the plasma edge, which causes a subsequent change in edge D_α and impurity light. Figure 11(c) shows the spectra acquired by the central FIDA channel across this event. Comparison of the spectrum acquired just before the sawtooth crash (3156 ms) with the spectrum acquired just after the crash (3157 ms) shows a clear reduction in signal for wavelengths that correspond to vertical energies of 30–80 keV. However, the subsequent spectra (3158 and 3159 ms) show that the impurity lines (and presumably the contribution from scattered D_α light) rise steadily as the heat pulse reaches the plasma edge.

The impact of various background-subtraction techniques is illustrated in Fig. 11(d) for the time slice at 3159 ms. If one uses the beam-modulation technique to correct the background, residual impurity lines appear in the spectrum; also, for wavelengths that correspond to vertical energies greater than the injection energy, the signal is larger than zero, indicating contamination by scattered cold D_α light. In contrast, the procedure for correction of dynamic

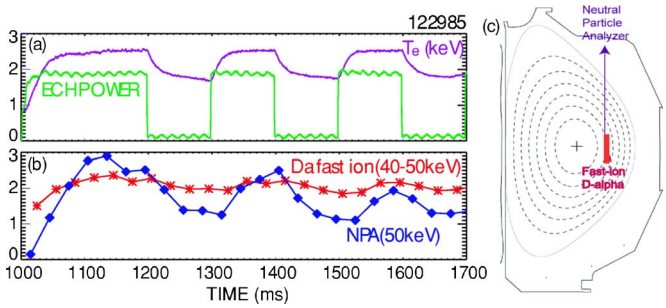

FIG. 12. (Color online) Time evolution of (a) ECH power and electron temperature and (b) NPA signal at 50 keV and the FIDA signal integrated over 40–50 keV. (c) The viewing geometry of the NPA and the spatial location of the FIDA measurement.

changes in background gives reasonable results. The impurity lines are successfully removed by fitting. Application of Eq. (9) makes the background above the injection energy close to zero and lowers the inferred fast-ion contribution to the signal but has a little effect on the portion of the spectrum dominated by thermal ions. The temporal evolution obtained by this background subtraction technique is also reasonable [Fig. 11(b)]. If the average background obtained from beam modulation is employed, the inferred FIDA signal drops at the sawtooth crash but then instantly bounces back. This result is unphysical: previous measurements with, for example, neutron tomography[15] show that the fast-ion population recovers on the much slower time scale associated with beam fuelling. In contrast, with the dynamic background subtraction model, the signal from both channels drops and stays suppressed. The central FIDA channel drops by a factor of 2, while the FIDA channel that is just inside of the $q=1$ surface drops ~20%, which is consistent with the expected redistribution of fast ions. Prior to the sawtooth crash, when the signals are expected to be approximately constant in time, the variations are smaller with the beam-modulation technique but, overall, dynamic background subtraction is clearly superior.

The data of Fig. 11 prove that the FIDA diagnostic can observe changes in the fast-ion density on a 1 ms time scale.

This diagnostic measures the vertical velocity component of fast ions because we use vertical views. Fast ions are born with an initial pitch angle and energy. Coulomb collisions with electrons and ions result in deceleration and pitch angle scattering of fast ions. Since the vertical velocity is a component of the perpendicular velocity and the fast ions are born with substantial parallel energy, pitch angle scattering enhances the FIDA signal level in the high energy range by increasing the perpendicular energy of fast ions. The slowing down time of fast ions on electrons is proportional to $T_e^{3/2}$ (T_e denotes electron temperature). Higher T_e means a longer slowing down time and more pitch angle scattering. To study the dependence of the FIDA signal on T_e, modulated electron cyclotron heating (ECH) power is added to a discharge with steady neutral beam injection. As shown in Fig. 12(a), the ECH heats electrons and modulates T_e. Figure 12(b) shows that, as expected, the FIDA signal increases and decreases with electron temperature. Active charge exchange data from a vertically viewing neutral particle analyzer[16] (NPA) are strongly modulated by the change in T_e. As illustrated in Fig. 1(a), the NPA detects fast ions from a much smaller volume of velocity space than the FIDA diagnostic, so it is much more sensitive to changes in the pitch angle distribution than FIDA.

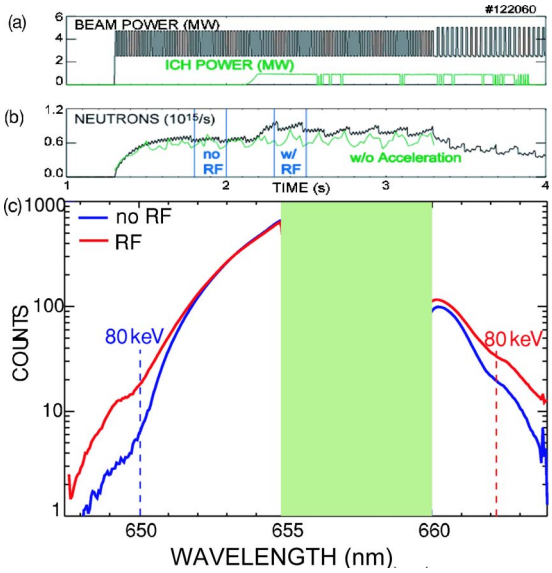

FIG. 13. (Color online) Time evolution of (a) beam power and ICH power and (b) the neutron rate. The green line is the calculated neutron rate assuming no acceleration of fast ions by the ICH. The time windows before and during the rf for FIDA analysis are also shown. (c) FIDA spectra before and during the rf. The two dashed lines denote the injection energy (80 keV).

FIDA is an excellent diagnostic to observe fast-ion acceleration by ion cyclotron heating (ICH) because it measures the vertical component of perpendicular energy, which increases during ICH. As shown in Fig. 13(b), after the fourth harmonic ICH is turned on, the neutron rate increases substantially, which is an indication of fast-ion acceleration.[17] Figure 13(c) shows the spectrum before and after the ICH is turned on. Strong acceleration beyond the injection energy is observed, and percentagewise fast ions with higher perpendicular energy are accelerated more, which agrees with theory. The symmetric nature of the spectrum is expected because of the gyromotion of fast ions.

VII. IMPLICATIONS

The success of the FIDA diagnostic is based on the vertical views, the blocking bar, beam modulation, and the high quantum efficiency detector. The vertical views separate the fast-ion signal from the bright interferences from other neutrals by taking advantage of the gyromotion of fast ions. The vertical bar on the exit focal plane of the spectrometer blocks the portion of spectrum contaminated by strong interferences to avoid camera saturation. The viewed beam is modulated to do background subtraction, which removes visible bremsstrahlung, most scattered light, and some impurity lines. The high quantum efficiency of the CCD camera provides a good signal to noise ratio. For future upgrades and implementations, the following possible improvements and alternatives should be considered.

Vertical views are chosen for the present diagnostic to minimize the Doppler shift for injected neutral emission;

however, they are not the only options. An alternative view is a tangential view on the midplane that is perpendicular to the neutral beam. The advantage of this view over vertical views is that the signal would be much stronger (especially in the large Doppler shift range) because there is less pitch angle scattering required after the fast-ion birth. In devices with low electron temperature, this view would make a big difference on signal levels.

The present system can only measure two chords simultaneously. It is essential to have more views to provide a full spatial profile. The chords should view the neutral beam from the magnetic axis to the outer edge. Although the fast-ion density is much lower in the plasma edge, the higher injected neutral density makes the FIDA signal comparable to that of central chords. The spatial interval between neighboring chords should be larger or approximately equal to the intrinsic spatial resolution. The best way to accommodate multiple spectra on a CCD chip depends on the temporal resolution requirement. For a temporal resolution of ~ 1 ms, a sufficiently fast mechanical shutter is unavailable. To prevent image smearing, at most four spectra can be put on the existing CCD chip with one on each quadrant (assuming each spectrum can be shrunk to half of the CCD width). For a temporal resolution of ~ 10 ms, a chopper wheel can be used to shade the CCD during frame transfer, allowing more spectra on a CCD chip. The maximum number of chords for a single CCD camera is determined by CCD chip size, fiber size, and dispersion of the system. For a certain camera, on-chip binning can be applied to improve the readout speed. Pixels can be binned vertically for each chord since they do not contain any useful information. Pixels in the serial direction correspond to different wavelengths. Since the FIDA diagnostic only has a rough spectral resolution, pixels in the serial direction can be binned to a large extent if necessary. The on-chip binning allows us to achieve good temporal resolution even with a modest speed camera.

Beam modulation is a good technique for background subtraction; however, when there is a dynamic background change, the background subtraction is problematic. A solution is to use separate background sight lines that miss the neutral beam and have the same viewing geometry as the beam viewing sight lines. These background sight lines allow dynamic background subtraction for the FIDA measurement. Scattering appears to be on a significant level for the present system. There are three possible sources: the spectrometer, the blocking bar, and the camera lenses. It is desirable to have a spectrometer with less scattering and a blocking bar covered with more absorbent material.

To increase the signal level over the present system, the most effective way is to equip the system with a low f/number collection lens. For example, a $f/1.8$ collection lens would increase the signal by a factor of 6 compared to a $f/4.4$ collection lens. Many of these ideas are incorporated in the FIDA diagnostic that is planned for installation on NSTX.[18]

ACKNOWLEDGMENTS

The assistance of R. Boivin, W. Solomon, J. Lynch, J. Kulchar, W. Carrig, D. Thomas, C. Hsieh, D. Finkenthal, N. Brooks, E. Ruskov, R. Groebner, E. Strait, M. Wade, and the entire DIII-D team is gratefully acknowledged. This work was supported by the U. S. Department of Energy Subcontract No. SC-G903402 and Contract No. DE-FC02-04ER54698.

[1] W. W. Heidbrink and G. J. Sadler, Nucl. Fusion **34**, 535 (1994).
[2] I. H. Hutchinson, *Principles of Plasma Diagnostics* (Cambridge University Press, New York, 1987).
[3] R. C. Isler, Phys. Rev. Lett. **38**, 1359 (1977).
[4] M. G. Von Hellermann, W. G. F. Core, J. Frieling, L. D. Horton, R. W. T. Konig, W. Mandl, and H. P. Summers, Plasma Phys. Controlled Fusion **35**, 799 (1993).
[5] G. R. Mckee *et al.*, Phys. Rev. Lett. **75**, 649 (1995).
[6] W. W. Heidbrink, K. H. Burrell, Y. Luo, N. A. Pablant, and E. Ruskov, Plasma Phys. Controlled Fusion **46**, 1855 (2004).
[7] Y. Luo, W. W. Heidbrink, and K. H. Burrell, Rev. Sci. Instrum. **75**, 3468 (2004).
[8] M. G. Von Hellermann *et al.*, Rev. Sci. Instrum. **61**, 3479 (1990).
[9] J. Egedal and H. Bindslev, Phys. Plasmas **11**, 2191 (2004).
[10] D. M. Thomas, K. H. Burrell, R. J. Groebner, P. Gohil, D. Kaplan, C. Makariou, and R. P. Seraydarian, Rev. Sci. Instrum. **68**, 1233 (1997).
[11] http://cow.physics.wisc.edu/~craigm/idl/fitting.html
[12] K. Levenberg, Q. Appl. Math. **2**, 164 (1944).
[13] D. W. Marquardt, J. Soc. Ind. Appl. Math. **11**, 431 (1963).
[14] W. Mandl, Ph.D. thesis, JET, 1992.
[15] F. B. Marcus *et al.*, Plasma Phys. Controlled Fusion **33**, 277 (1991).
[16] E. M. Carolipio and W. W. Heidbrink, Rev. Sci. Instrum. **68**, 304 (1997).
[17] W. W. Heidbrink, E. D. Fredrickson, T. K. Mau, C. C. Petty, R. I. Pinsker, M. Porkolab, and B. W. Rice, Nucl. Fusion **39**, 1369 (1999).
[18] W. W. Heidbrink, R. E. Bell, Y. Luo, and W. Solomon, Rev. Sci. Instrum. **77**, 10F120 (2006).